CrystEngComm

ROYAL SOCIETY OF CHEMISTRY

PAPER

Cite this: *CrystEngComm*, 2023, **25**, 2557

Competing and directing interactions in new phosphoramide/thiophosphoramide structures: energy considerations and evidence for CH···HC contacts and aliphatic–aromatic stacking†

Saeed Hosseinpoor, [a] Mehrdad Pourayoubi, *[a] Mozhgan Abrishami,[b] Marjan Sobati,[b] Fatemeh Karimi Ahmadabad, [a] Fahimeh Sabbaghi,[c] Marek Nečas,[d] Michal Dušek, [e] Monika Kučeráková[e] and Manpreet Kaur[f]

Received 3rd March 2023,
Accepted 16th March 2023

DOI: 10.1039/d3ce00204g

rsc.li/crystengcomm

Supramolecular aggregates, driven by different molecular functionalities and crystal forces, are studied in new phosphoramide and thiophosphoramide structures $(C_6H_5O)_2P(O)(2\text{-}NHC_5H_4N)$ (**I**), $(4\text{-}Cl\text{–}C_6H_4O)P(O)(NHC_6H_{11})_2$ (**II**), $(4\text{-}Cl\text{–}C_6H_4O)P(O)(N(CH_3)C_6H_{11})_2$ (**III**), $P(S)(NHC(CH_3)_3)_3$ (**IV**), and $P(S)(3\text{-}NHC_5H_4N)_3$ (**V**). DH···A (D = N, C; A = N, O, S) hydrogen bonds, contacts related to the ring stacking (CH···π/σ···π and π···π) and some other weak interactions are the structural elements inspected. The techniques/methods used are X-ray crystallography, QTAIM, NCI, 2D fingerprint plots, and lattice energy calculations, complemented by spectroscopic approaches for some additional investigations. A comparison is made with selected analogous structures from the Cambridge Structural Database (CSD). Determinative roles of stronger hydrogen bonds and competition between weaker hydrogen bonds (mostly having dispersion characteristics) are addressed as well as the cyclohexyl···arene (σ···π) stacking with pronounced CH···π interactions. When the strength and specificity of the hydrogen bonds decrease, the molecules can form a denser packing, and the role of CH···HC interactions becomes prominent. Despite their weakness, such interactions together make the bulk of the crystal stabilizing forces.

Introduction

Some structural features of non-covalent interactions, including geometry, strength, contribution to the hydrogen bond motif/pattern, and the way of their characterization as well as their possible role in the crystallization process, were studied.[1,2] In the nucleation stage of crystallization, the competition between the elements constituting these interactions can determine the primary aggregation arrangement.[3,4] In the growth stage, the formed pattern may continue until the formation of mature crystals (kinetic product), but it is often rearranged to a more stable phase (thermodynamic product),[5] in which the crystal lattice energy is generally greater.

Among intermolecular interactions, the ones with electrostatic nature, like moderate to strong hydrogen bonds (HBs) and σ-hole interactions, usually have priority compared to others, since raising the strength of such an interaction increases the tendency of stability, both in the primary aggregate and final crystal structure. Thus, predicting the probable patterns based on electrostatic interactions has become a useful way of predicting supramolecular assembly,[6] and crystal engineers have studied the participation of such interactions, especially in the stronger contacts, for many years.[7–9]

On the other hand, a London dispersion force (usually referred to as the dispersion interaction), although singly has low strength, in many organic crystals, totally makes up the major share of crystal lattice energy. In molecules with low electrostatic potentials, the role of dispersion interactions is significant,[10,11] and even if HBs form specific patterns, these interactions play an influential role in the arrangement of the molecules in some segments and directions.[12]

[a] *Department of Chemistry, Faculty of Science, Ferdowsi University of Mashhad, Mashhad, Iran. E-mail: pourayoubi@um.ac.ir*
[b] *Department of Chemistry, Payame Noor University, 19395-4697 Tehran, Iran*
[c] *Department of Chemistry, Zanjan Branch, Islamic Azad University, Zanjan, Iran*
[d] *Department of Chemistry, Masaryk University, Kotlarska 2, Brno, 61137, Czech Republic*
[e] *Institute of Physics of the Czech Academy of Sciences, Na Slovance 2, 182 21 Prague 8, Czech Republic*
[f] *Department of Chemistry, Keene State College, Keene, NH, USA*

† Electronic supplementary information (ESI) available. CCDC 2207982, 2207985–2207987 and 1405631. For ESI and crystallographic data in CIF or other electronic format see DOI: https://doi.org/10.1039/d3ce00204g

The most studied interactions with high dispersion characters are π···π and C–H···π, which have a great impact on the packing of aromatic ring-containing molecules. Further research shows the significance of other types of dispersion interactions, typically homopolar H···H interactions in which their energies were estimated using quantum theory of atoms in molecules (QTAIM) calculations.[13] Although this type of interaction is usually very weak on its own, a large number of C–H units in organic compounds can make them important. Subsequent studies showed that such interactions between two cyclohexane molecules (namely σ···σ stacking[14]) are computed to be even stronger than π···π stacking between two benzene molecules.[15] However, in π-systems, the rate of increase in interaction energy related to the increase in system size is much greater than in saturated systems, owing to the delocalized π-effect. This was shown in tighter calculated stacking between the graphene than graphane sheets with different nano-sizes.[15–17]

Phosphoramides/thiophosphoramides have been known for their wide applications as drugs,[18] pesticides,[19] and coordinating ligands.[20,21] They can be defined with the general formula P(X)(NR^{1}R^2)(R^3)(R^4) (X = O, S; R^1/R^2 = hydrogen or any organic group and R^3 and R^4 = alkoxy/aryloxy, amine/amide, or even halogen/hydroxyl). The synthetic methods available allow the preparation of a variety of such compounds with different substituents and the design of the target molecules with different types of interactions in the crystal structures. The HB patterns/strengths in these structures usually have been considered by researchers,[22,23] but in most cases, the roles of other types of interactions have not been discussed.

In the present work, we report five new structures belonging to the phosphoramide and thiophosphoramide families (Chart 1) to study different moderate to weak contacts. The compounds were chosen to have different interactions in the crystal structures, including D–H···A (D = N, C; A = N, O, S) HBs, and contacts related to the ring stacking (C–H···π/σ···π, and π···π). Through energy consideration, the role and participation rate of individual interaction in the packing, as well as the energy components, are investigated. The crystal lattice energy calculations, combined QTAIM/non-covalent interaction (NCI) analysis, and 2D fingerprint plots were applied. Crystal packing features are described, and the significance of each type of interaction is discussed using a database survey and comparison of new structures reported here and selected analogous structures retrieved from the Cambridge Structural Database (CSD).

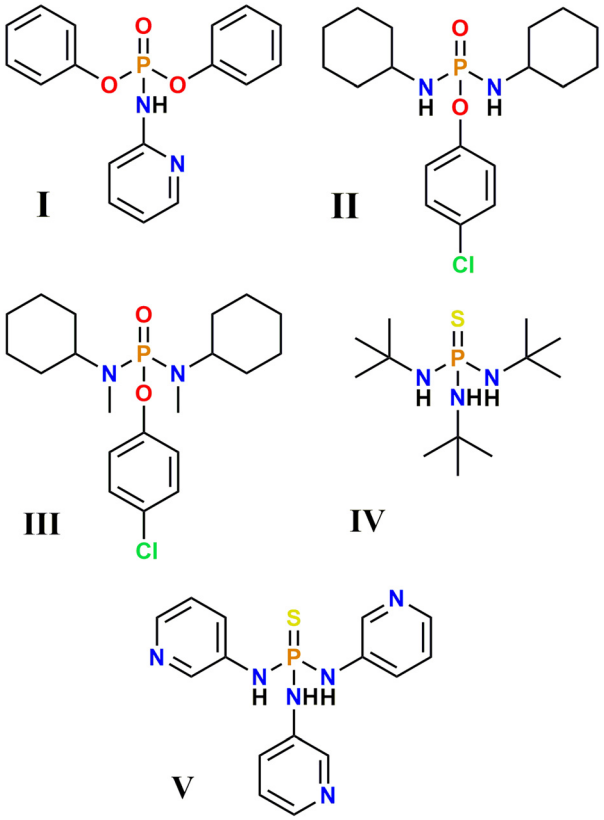

Chart 1 Chemical structures of I–V.

Results and discussion

Crystal structure description based on energy calculations

In all of the structures **I–V**, the asymmetric unit consists of one complete molecule (Fig. S1–S5†). The P atoms have a distorted tetrahedral environment in different P(O)NO_2, P(O)N_2O, and P(S)N_3 skeletons, and the P═O, P═S, P–N, and P–O bond lengths are within the normal ranges of the analogous structures.[24,25] A cocrystal of compound **V** with methanol solvent is previously reported[26] (Refcode: RECMUK). The conformation of thiophosphoramide molecules in these two structures is almost similar, and the only significant difference is the rotation of one ring (about 180°) reflected in the position of the pyridine N atom (N3). X-ray crystal data and structure refinement details of compounds **I–V** are given in Table 1, and selected bond lengths and angles, and hydrogen bond geometry parameters are given in Tables S1–S10.† The interaction energies for all molecular pairs of structures **I–V** are given in Tables S11–S15.†

In structure **I**, the $N_{pyridyl}$ is a successful acceptor (in competition with P═O) to interact with the only existing NH unit, while the P═O group takes part in the CH unit in hydrogen bonding. For molecular pairs with E_{tot} < −20 kJ mol^{-1} centrosymmetric dimers are formed. The dimer synthon with the highest total energy, shown as ***Ia***, includes 2 × NH···N and 2 × CH···O═P HBs (Fig. 1, E_{tot} = −79.2 kJ mol^{-1}). In the crystal, the connection of such dimers with dimers ***Ib*** and ***Ic*** constructs a sheet parallel to the (011) plane. The most important interactions in ***Ib*** and ***Ic*** are CH···OP HBs, and both types of oxygen atoms in the O–P═O moiety take part in hydrogen bonding. The stacking of sheets to construct a three-dimensional network happens through

Table 1 Crystallographic parameters of structures I–V

	I	II	III	IV	V
Empirical formula	$C_{17}H_{15}N_2O_3P$	$C_{18}H_{28}ClN_2O_2P$	$C_{20}H_{32}ClN_2O_2P$	$C_{12}H_{30}N_3PS$	$C_{15}H_{15}N_6PS$
Formula weight	326.28	370.9	398.9	279.42	342.36
Temperature (K)	173	120	293	120	120
Wavelength (Å)	0.71073	1.54184	1.54184	0.71073	0.71073
Crystal system	Triclinic	Monoclinic	Monoclinic	Orthorhombic	Orthorhombic
Space group	$P\bar{1}$	$P2_1/c$	$P2_1/c$	$Pna2_1$	$Pna2_1$
a (Å)	9.0129 (7)	11.2653 (2)	6.0515 (2)	11.1802 (6)	9.4456 (2)
b (Å)	10.0163 (7)	19.0533 (4)	17.9235 (8)	9.6493 (6)	12.1063 (2)
c (Å)	10.4720 (7)	8.9226 (2)	19.3040 (8)	15.1332 (8)	14.6424 (3)
α (°)	64.525 (7)	90	90	90	90
β (°)	76.954 (6)	99.3906 (19)	93.157 (3)	90	90
γ (°)	66.104 (7)	90	90	90	90
V (Å^3)	778.78 (11)	1889.49 (7)	2090.61 (14)	1632.59 (16)	1674.38 (6)
Z	2	4	4	4	4
D_{calc} (Mg m^{-3})	1.391	1.304	1.267	1.137	1.358
μ (mm^{-1})	0.19	2.69	2.47	0.28	0.30
F(000)	340	792	856	616	712
Crystal size (mm)	0.4 × 0.28 × 0.26	0.43 × 0.26 × 0.11	0.50 × 0.24 × 0.15	0.25 × 0.25 × 0.20	0.20 × 0.20 × 0.10
T_{min}, T_{max}	0.847, 1	0.289, 1	0.626, 1	0.762, 1	0.851, 1
R_{int}	0.027	0.032	0.053	0.043	0.024
$(\sin\theta/\lambda)_{max}$ (Å^{-1})	0.762	0.598	0.598	0.602	0.602
R^a	0.043	0.031	0.051	0.036	0.025
w$R(F^2)$	0.116	0.054	0.063	0.091	0.064
S^b	1.04	2.12	1.62	1.06	1.05
No. of reflections	5069	3385	3644	2896	2985
No. of parameters	213	223	235	164	208
$\Delta\rho_{max}$, $\Delta\rho_{min}$ (e Å^{-3})	0.36, −0.33	0.26, −0.25	0.35, −0.37	0.34, −0.24	0.17, −0.24

[a] The observability limit are $I > 2\sigma(I)$ for **I**, **IV**, and **V**, and $I > 3\sigma(I)$ for **II** and **III**. [b] The program Jana2006 used to refine **II** and **III** does not adjust the weighting scheme. Therefore, S based on the experimental weights retains its original meaning. Such S is always above 1 when the crystallographic model uses spherical form factors and good-quality data sets.

the interactions shown in pairs **Id**, **Ie**, and **If**. Pairs **Id** and **Ie** comprise C–H···π and π···π interactions with an E_{tot} of −31.2 and −28.9 kJ mol^{-1}, respectively, and the pair **If** is formed through 2 × C–H···O═P HBs and a weak H···H contact.

Considering classical HB, structure **II** comprises one acceptor and two donor sites, forming the (N–H)$_2$···O═P grouping (pair **IIa**, Fig. 2) and repeating it in a one-dimensional chain along the *c*-axis. The QTAIM/NCI plot shows that several other interactions (C–H···O, H···H, C–H···N, C–H···Cl, and C–H···π) strengthen this molecular pair, resulting in a total energy of −99.8 kJ mol^{-1}. The neighboring chains are stacked by C–H···X (X = O═P, π), H···H, and π···π interactions, shown in pairs **IIb**, **IIc**, and **IId**, in a two-dimensional array along the *bc*-plane.

Structure **III** lacks an N–H group, and weak interactions contribute to the crystal packing. The more effective interactions are seen along the *a*-axis, which include two C–H···O═P HBs, and some C–H···H–C interactions with a total energy of −52.4 kJ mol^{-1} (Fig. 2, pair **IIIa**). In the two other directions (*b* and *c*), the C–H···Cl, C–H···π, and C–H···H–C interactions are present (pairs **IIIb** and **IIIc** with E_{tot} = −30.5 and −31.2 kJ mol^{-1}). A notable feature of this structure is the parallel ordering of cyclohexyl rings (pair **IIIa**), which causes the formation of additional C–H···H–C interactions.

The only strong molecular pair of structure **IV** includes an N–H···S═P, multiple C–H···S═P, and C–H···H–C interactions (Fig. 3, pair **IVa**, E_{tot} = −44.9 kJ mol^{-1}), which propagates through a linear arrangement along the *a*-axis. The other pairs (including several C–H···H–C interactions) have weaker energies than −20 kJ mol^{-1}. Nevertheless, the energy sum of these weak interactions is equal to −69.7 kJ mol^{-1} and makes up 60.8% of the calculated lattice energy (E_{latt} = −114.6 kJ mol^{-1}).

In structure **V**, different orientations of the N atoms of three pyridine rings lead to the formation of three pairs containing N–H···N HBs with E_{tot} < −20 kJ mol^{-1}, and a three-dimensional HB pattern as a result. Besides, N–H···S═P, C–H···π, and C–H···H–C interactions reinforce the stabilization of this assembly, as can be seen in Fig. 3. The calculated lattice energy equals −201.3 kJ mol^{-1} and interaction energies of pairs **Va**–**Vc** comprise 82.5% of it.

Analyses of fingerprint plots

Two-dimensional fingerprint plots are used to explore detailed information on intermolecular interactions in crystals. The percentages of contacts in the structures **I** to **V** (Fig. 4) indicate the highest participation between hydrogen atoms. An increase of H···H contact participation was observed with the addition of alkyl substituents to a molecule instead of arene groups, and the highest percentage belongs to structure **IV**. The percentage of C···H contacts is related to the presence and number of aromatic rings.

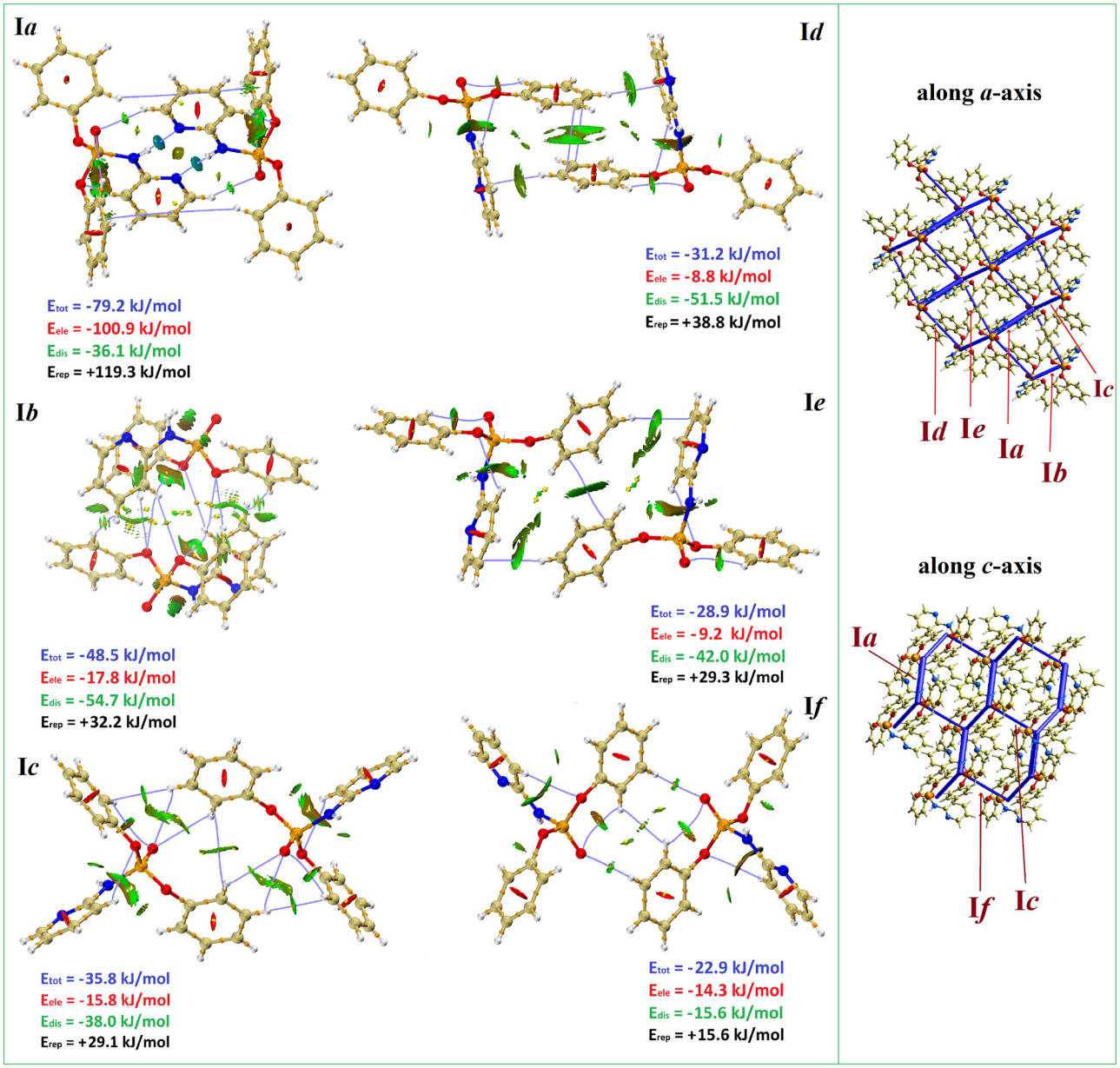

Fig. 1 The combined QTAIM/NCI plots of the molecular pairs in structure **I**, with $E_{tot} < -20$ kJ mol^{-1} (atom color codes: P = orange, O = red, N = blue, C = light beige and H = white). The total energies and their components are listed (left). The energy framework of structure **I** (cutoff energy value = −20 kJ mol^{-1}) along the *a*-axis (top) and *c*-axis (down) (right).

The lowest $d_i + d_e$ value for H···H contacts is seen in structure **II**, which is related to a contact between the phenyl and cyclohexyl rings (pair **IIc**, Fig. 2, H···H distance = 2.30 Å). Distinctive spikes in the fingerprint plots correspond to the strongest hydrogen bonding in the structure, as are seen for N–H···$N_{pyridyl}$ (**I** & **V**, label 1), N–H···O═P (**II**, label 2), and C–H···O═P (**III**, label 2). The closest N–H···$N_{pyridyl}$ contact is seen in pair **Vc**, which has the lowest $d_i + d_e$ value (≈ 1.8). The H···O═P HB in structure **II** is stronger than that in **I** and **III**, reflected in the lower value of $d_i + d_e$ in **II** (≈ 1.9 *vs.* 2.1–2.4). The N–H···S═P HBs in structures **IV** and **V** reveal two wings in $d_i + d_e \geq 2.8$ (label 3). Apart from structure **IV**, the C···H interactions are seen on two sides of the plots (label 4). In structures **II** and **III**, these contacts in combination with H···Cl make two wings on the two sides of the plots (labels 4 and 6). In the plot of **I**, C···C contacts in the region with d_i and d_e equal to 1.7–1.9 show the π···π stacking of the arene rings.

Energy components and participation rate of different interactions

The contributing impacts of the most important interactions on the crystal lattice energy are now analyzed. For this purpose, topological parameters obtained from QTAIM analysis (Table 2), and results of lattice energy calculations of

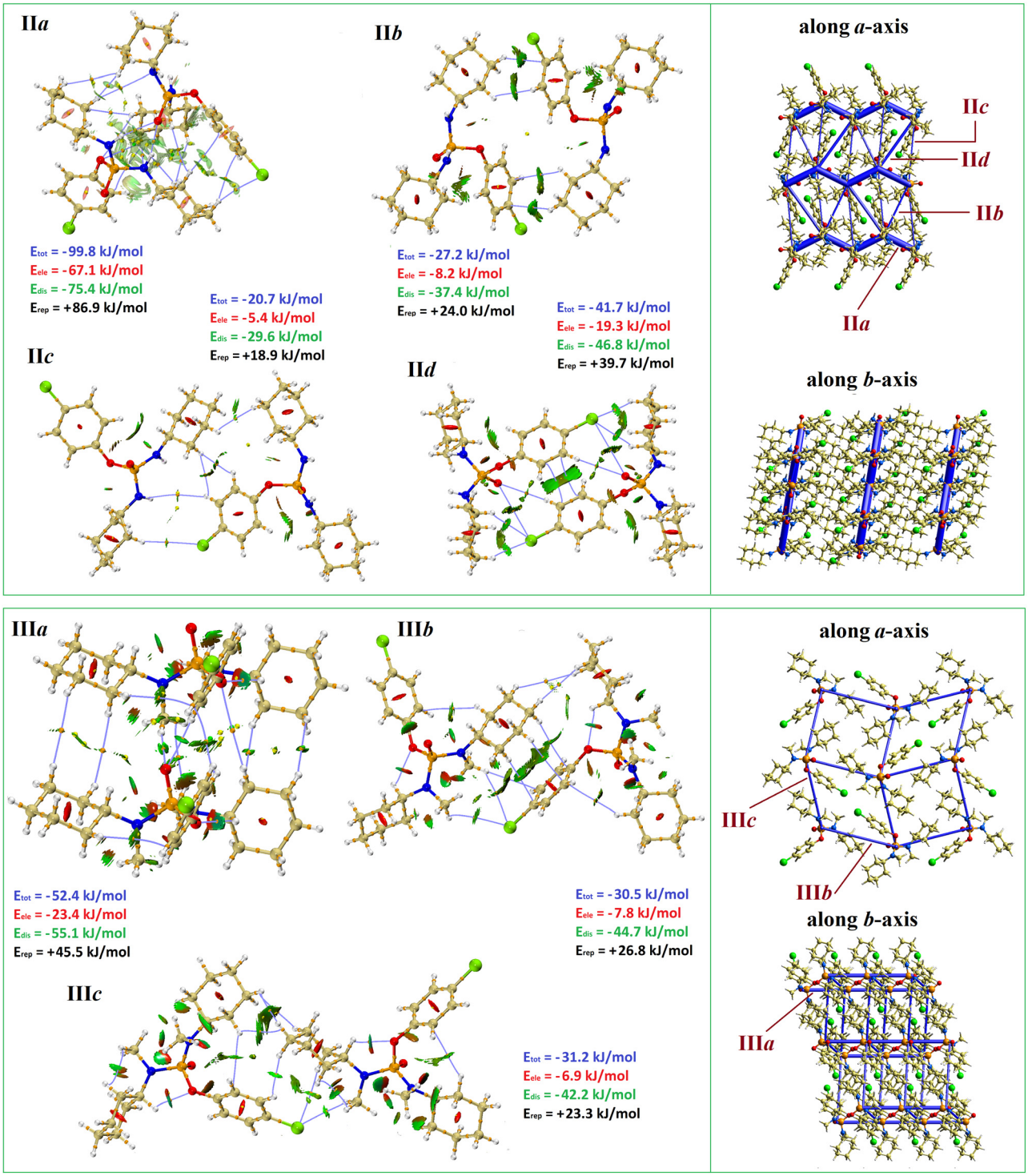

Fig. 2 The combined QTAIM/NCI plots of the molecular pairs in structures II and III, with $E_{tot} < -20$ kJ mol^{-1} (atom color codes: P = orange, O = red, N = blue, C = light beige, Cl = light green and H = white). The total energies and their components are listed (left). The energy frameworks of structures II and III (cutoff energy values = −20 kJ mol^{-1}) along the *a*-axis and *b*-axis (top and down in the related frame of each structure) (right).

new structures and three CSD structures are considered (Fig. 5). The QTAIM analysis were carried out at M06-2X/6-311G and M06-2X/6-311++G levels of theory, and the results are almost the same, except for the weak CH···Cl and CH···N interactions in pairs **III*c*** and **V*c***. The discussion was made by higher-level calculation (Tables 2 and S16†) and other data were also presented for comparison (Tables S17–S19†). Following, the contribution of hydrogen bonds, π-interactions, CH···HC contacts, and repulsion forces are detailed.

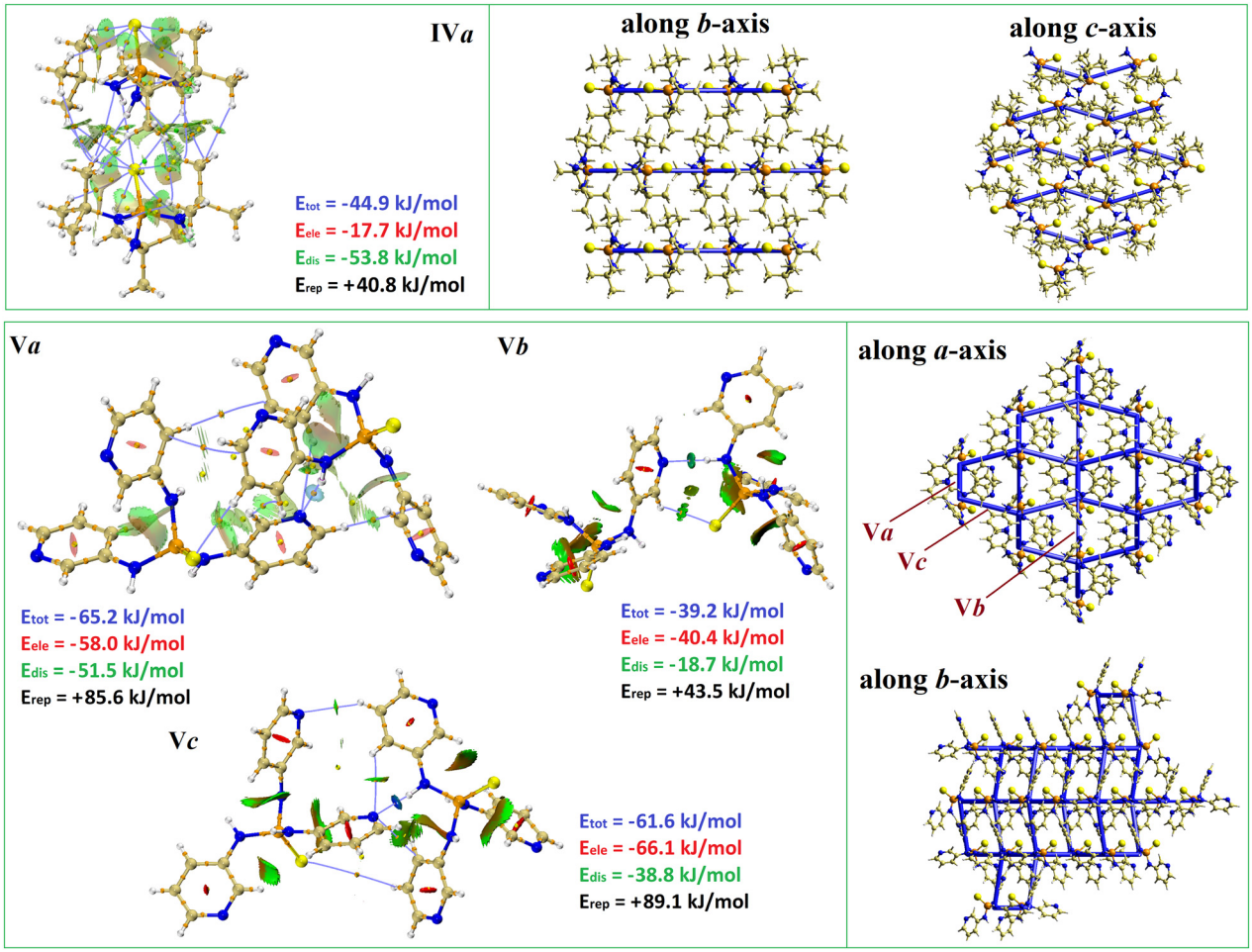

Fig. 3 The combined QTAIM/NCI plots of the molecular pairs in structures **IV** and **V**, with $E_{tot} < -20$ kJ mol^{-1} (atom color codes: P = orange, S = yellow, N = blue, C = light beige, and H = white). The total energies and their components are listed (left). The energy frameworks of the structures **IV** and **V** (cutoff energy values = −20 kJ mol^{-1}) are represented along the *b*- and *c*-axis, and *a*- and *b*-axis, respectively (right).

Hydrogen bonds. In the phosphoramide structures, the highest electrostatic interactions are related to the pairs that include N–H (donors) taking part in HB interactions with N (pyridine) and/or O (P═O) atoms (acceptors). Regardless of structure **V**, the share of electrostatic interactions in lattice energy is lower than that of dispersion; however, in all structures, the role of the strongest HBs is determinative in constructing the molecular assembly. In the structures in question, wherever the NH group exists, it cooperates with an acceptor with a high acceptor capability to form a classical HB. Thus, such an acceptor directs the HB motif. In these structures, the total energy of the molecular pair constructed from the main H-bond interaction has the highest value, which arises from the synergistic effect of HB with dispersion interaction.

Following what was mentioned, most energy values are related to the pairs constructed from the N–H···N$_{pyridyl}$ (**V*a***, **I*a***, and **V*c***), (N–H)$_2$···O═P (**II*a***), N–H···S═P (**IV*a***), and C–H···O═P (**III*a***) HBs (Fig. 1–3, Table 2). The potential energy density values also confirm that the strongest interactions, between all of the studied, are N–H···N$_{pyridyl}$ with a $V(r)$ of −0.0336 and −0.0264 a.u. in pairs **V*c*** and **V*a***, and −0.0247 a.u. in **I*a***, manifested as the blue surfaces in the NCI plots. The strengths of interactions are reflected in the N···N distances, too (2.838 (3), 2.888 (3), and 2.9229 (16) Å, respectively). Pair **V*b*** has the weakest N–H···N$_{pyridyl}$ HB ($V(r)$ = −0.0155 a.u.) and the longest N···N distance (3.038 (2) Å). In structure **V**, the overall effect of three 3-NHC$_5$H$_4$N groups with high electrostatic potential causes not only maximization of the electrostatic contribution to the crystal lattice energy (44.3% of attractive energies) but also raises the crystal lattice energy compared to the other structures studied.

The (N–H)$_2$···O═P grouping in structure **II** comprises other types of moderate HBs with a high contribution to the crystal formation (pair **II*a***). However, it is expected to reduce the energies of two HBs received by the phosphoryl group due to the anti-cooperativity effect and repelling of two NH units together.[27] The $V(r)$ values are −0.0200 and −0.0146 a.u., and the hydrogen-bonded pair formed involves some other parts of the molecules with suitable proximity, too, which contribute to dispersion interactions.

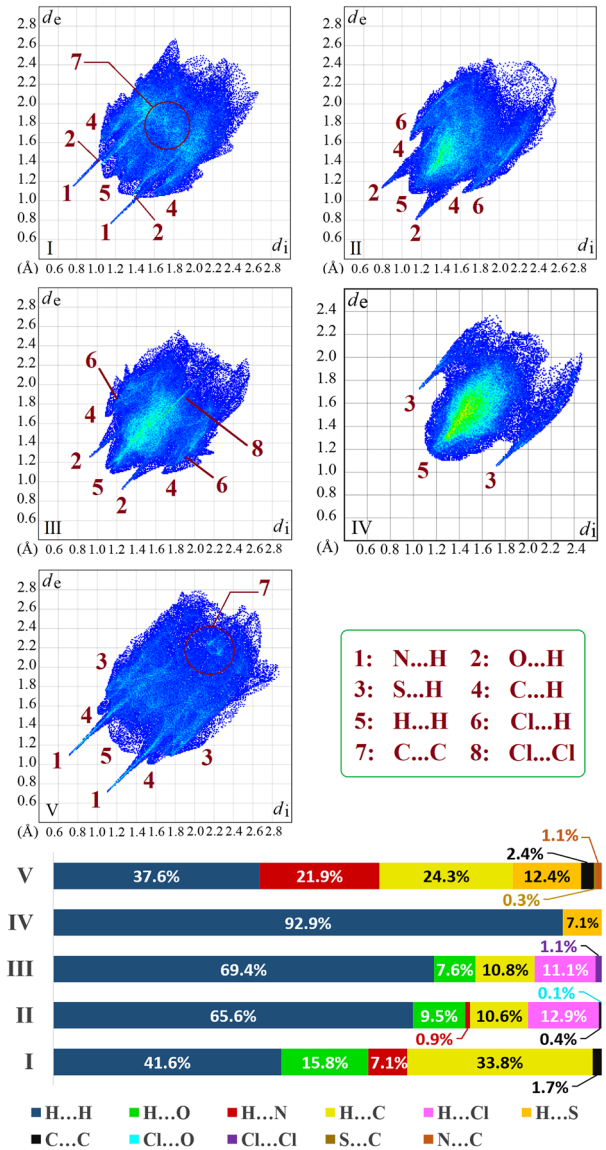

Fig. 4 2D fingerprint plots and percentages of contacts in structures I–V. The location of each contact is shown by the numbers on the plots.

The significance of weaker HBs almost decreases in the sequence of C–H···O═P, C–H···$O_{(ester)}$–P, N–H···S═P, C–H···S═P, and C–H···Cl. Structure **III** lacks any N–H group to form a moderate/strong HB; thus, the main HBs of the phosphoryl group are established with the hydrogen atoms of two CH units (from NCH_3 and arene fragments) with $V(r)$ values of −0.0066 and −0.0095 a.u.

In addition to the strongest HBs made by phosphoryl groups (appeared in pairs **Ia**, **IIa**, and **IIIa**), there are some weaker C–H···O═P in pairs **Ic**, **If**, and **IId** with $V(r)$ of −0.0034/−0.0039, −0.0053, and −0.0028 a.u., respectively.

Hydrogen bond interactions received by non-O/N atoms are weaker, and generally, their role is not determinative in the presence of these two acceptors. In the case of C–H···Cl HBs, this is evidenced by comparing the results of lattice energy calculations of **II** and the structure with refcode EVOSUE. These two crystal structures are very similar, except for the substituent attached to the arene ring, *i.e.*, chlorine in (**II**) and methyl in EVOSUE. The conformations of the molecules are similar (structure overlay is given in Fig. S6†), and the packing features are almost the same. The energy frameworks show almost similar shapes, but the energy values of equivalent pairs have some differences (Fig. S7†). For example, there is a remarkable difference between pair **IId** and its equivalent pair in EVOSUE (ΔE_{tot} = 5.8 kJ mol^{-1}, Table S20†). A closer look at the interactions shows that this is due to the HBs received by the chlorine atom (Fig. 2), which disappear upon replacement of the methyl group. In total, the attractive energies of structure **II** are higher, which correspond to the stronger interactions of the chlorine atom, but the repulsive forces almost neutralize their effect, and the difference between their crystal lattice energies is equal to 4.6 kJ mol^{-1}. Altogether, the observations represent that the role of the C–H···Cl HB is not determinative due to the lack of distinctive differences in the crystal packing. They just stabilize the formed arrangement.

***π*-Interactions.** π-Holding interactions, π···π, and CH···π mostly comprise the dispersion energy component. After the noted hydrogen bonds of the new structures, the π-interactions have the greatest effect on the crystal packing maps of **I**, **II**, and **III**. In structure **I**, a dimer is formed through a π···π stacking and two equal CH···π interactions with a total energy of −31.2 kJ mol^{-1} (Fig. 1, pair **Id**). There are some weaker π···π interactions in pairs **Ie** and **IId**, and CH···π interactions in pairs **Ic**, **Ie**, **IIa**, **IIb**, **IIIb**, and **IIIc**. If the two arene and cyclohexyl rings are facing each other (like pairs **IIb**, and **IIIb**, Fig. 2), as QTAIM/NCI plots demonstrate, the number and overall importance of CH···π interactions is enhanced. Indeed, with the smaller angle between the two rings (closer to the parallel position), the number of hydrogen atoms involved in the CH···π interactions increases. Recent studies have shown that these interactions, which are referred to as σ···π stacking, can even have higher strength than π···π ones.[28,29] For pairs **Id** and **IId**, broad surfaces in the NCI plots between the parallel arene rings show a combination of attractive (green) and repulsive (yellowish brown) forces. In pairs **Ic**, **Ie**, and **IIIa**, with the greater angles between the arene rings, the repulsion forces are not observed and only weak attractive forces are seen. In structure **V**, three pyridyl rings are not involved in π···π stacking, and also the contribution of the CH···π interactions is lower than the other structures. The dominance of hydrogen bonding over π-interactions imposes the orientation of pyridyl rings and the arrangement of molecules so that π-interactions are minimized.

CH···HC interactions. The CH···HC interaction is a type of weak dispersion force[30] that, although in many cases has little involvement in the crystal formation, in some structures has a significant contribution to the crystal lattice energy (especially in structures with large saturated hydrocarbon fragments).[31–33] Structure **IV**, with three *tert*-butylamine

Table 2 Topological parameters and estimated energies (E_{Esp}) for selected interactions in the different pairs of structures **I–V**, using the neutron-normalized structures

Hydrogen bonds/contacts	$\rho(r)$ (e Å^{-3})	$\nabla^2\rho(r)$ (e Å^{-5})	$G(r)$	$V(r)$	E_{Esp} (kJ mol^{-1})
I*a*					
CH···O═P^a	0.0100	0.0337	0.0073	−0.0062	−8.1
NH···N^a	0.0317	0.0967	0.0244	−0.0247	−32.4
I*b*					
CH···O^a	0.0083	0.0298	0.0064	−0.0053	−6.9
CH···O^a	0.0023	0.0099	0.0019	−0.0013	−1.7
CH···O^a	0.0038	0.0143	0.0030	−0.0024	−3.2
I*c*					
CH···π^a	0.0077	0.0223	0.0046	−0.0036	−4.8
CH···O═P^a	0.0056	0.0190	0.0041	−0.0034	−4.5
CH···O═P^a	0.0063	0.0223	0.0047	−0.0039	−5.1
I*d*					
CH···N(π)^a	0.0075	0.0231	0.0050	−0.0042	−5.5
π···π^a	0.0060	0.0144	0.0030	−0.0024	−3.2
I*e*					
CH···π^a	0.0077	0.0217	0.0046	−0.0037	−5.0
π···π	0.0046	0.0123	0.0025	−0.0019	−2.5
I*f*					
CH···O═P^a	0.0087	0.0309	0.0065	−0.0053	−6.9
II*a*					
NH···O═P	0.0193	0.0799	0.0173	−0.0146	−19.2
NH···O═P	0.0241	0.1040	0.0230	−0.0200	−26.3
CH···O	0.0044	0.0151	0.0032	−0.0026	−3.4
CH···O	0.0041	0.0158	0.0033	−0.0026	−3.4
CH···N	0.0037	0.0100	0.0022	−0.0019	−2.4
CH···N	0.0031	0.0088	0.0019	−0.0015	−2.0
CH···Cl	0.0034	0.0105	0.0021	−0.0016	−2.2
CH···π	0.0042	0.0115	0.0024	−0.0019	−2.5
CH···π	0.0052	0.0155	0.0032	−0.0025	−3.3
CH···π	0.0023	0.0062	0.0012	−0.0010	−1.2
II*b*					
CH···π^a	0.0076	0.0212	0.0046	−0.0039	−5.1
CH···π^a	0.0045	0.0121	0.0025	−0.0020	−2.7
II*c*					
CH···Cl	0.0026	0.0080	0.0016	−0.0011	−1.5
II*d*					
CH···Cl^a	0.0061	0.0202	0.0041	−0.0032	−4.2
CH···Cl^a	0.0073	0.0226	0.0046	−0.0036	−4.8
Cl···O^a	0.0022	0.0074	0.0014	−0.0009	−1.2
CH···O═P^a	0.0048	0.0165	0.0035	−0.0028	−3.7
π···π^a	0.0054	0.0145	0.0030	−0.0023	−3.0
III*a*					
CH···O═P	0.0146	0.0575	0.0119	−0.0095	−12.5
CH···O═P	0.0110	0.0353	0.0077	−0.0066	−8.7
III*b*					
CH···Cl	0.0036	0.0116	0.0022	−0.0016	−2.1
CH···Cl	0.0040	0.0122	0.0025	−0.0020	−2.6
CH···π	0.0073	0.0207	0.0045	−0.0038	−4.9
CH···π	0.0042	0.0113	0.0024	−0.0019	−2.5
CH···π	0.0053	0.0148	0.0031	−0.0025	−3.3
CH···π	0.0051	0.0140	0.0030	−0.0024	−3.2
III*c*					
CH···Cl	0.0031	0.0089	0.0018	−0.0013	−1.7
CH···Cl	0.0054	0.0171	0.0034	−0.0026	−3.4
CH···π	0.0036	0.0103	0.0021	−0.0016	−2.1
IV*a*					
NH···S═P	0.0079	0.0236	0.0049	−0.0039	−5.1
CH···S═P	0.0046	0.0132	0.0027	−0.0020	−2.6
CH···S═P	0.0054	0.0151	0.0031	−0.0025	−3.2
V*a*					
NH···N	0.0329	0.1039	0.0262	−0.0264	−34.6
CH···N	0.0085	0.0248	0.0054	−0.0046	−6.0
CH···S═P	0.0057	0.0184	0.0037	−0.0027	−3.6
CH···π	0.0065	0.0176	0.0037	−0.0030	−4.0
CH···π	0.0069	0.0227	0.0046	−0.0036	−4.7

Table 2 *(continued)*

Hydrogen bonds/contacts	$\rho(r)$ (e Å^{-3})	$\nabla^2\rho(r)$ (e Å^{-5})	$G(r)$	$V(r)$	E_{Esp} (kJ mol^{-1})
V*b*					
NH···N	0.0230	0.0779	0.0175	−0.0155	−20.4
CH···S═P	0.0087	0.0242	0.0051	−0.0041	−5.3
V*c*					
NH···N	0.0388	0.1120	0.0308	−0.0336	−44.1
CH···N	0.0073	0.0223	0.0049	−0.0042	−5.5
CH···N	0.0081	0.0238	0.0051	−0.0042	−5.6
C(π)···N	0.0046	0.0147	0.0031	−0.0024	−3.2

[a] There are two equivalent such interactions in the molecular pair.

substituents, has the highest percentage of H···H contacts (= 92.9%), which also have the highest energy contribution to the total energy; similar contacts are more pronounced in **II** and **III** than in **I** and **V**. However, the pairs with the highest interaction energies are still formed along the direction of hydrogen bonding. QTAIM plots of the pairs having the H···H interactions (structures **I–IV**) and their topological parameters are given in Fig. S8 and Tables S17 and S18,† respectively.

According to QTAIM/NCI plots, wherever the aliphatic rings are parallel to each other, the bond paths and attractive surfaces are formed (pair **III*a***), similar to what was noted for π···π interactions. The smaller values of $V(r)$ and the color of surface areas show the weaker strengths of σ···σ relative to π···π interactions.

Here, it is noteworthy to consider if homopolar H···H interactions may have a determinative role in the formation of crystals of phosphoramide/thiophosphoramide structures. For this purpose, two thiophosphoramide structures with tertiary nitrogen atoms were selected from the Cambridge Structural Database (CSD)[34] to calculate the lattice energies (Chart 2; the data of energies are given in Tables S21 and S22†).

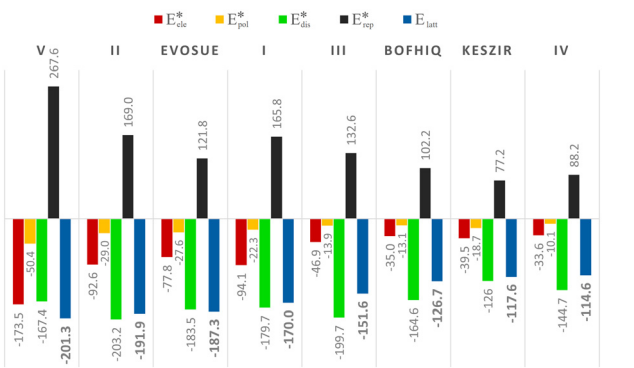

Fig. 5 Calculated crystal lattice energies and the sum of energy components for I–V and three selected analogous structures retrieved from the CSD. Red, yellow, green, black, and blue columns show the values of electrostatic, polarization, dispersion, repulsion (components), and lattice energies, respectively. The chart was sorted according to the lattice energy.

The reasons for the selection of these two structures[35,36] are (i) the low electrostatic potentials of both HB donor (C–H groups) and acceptor (sulfur atom) sites, which are expected to minimize the strengths of HBs, and (ii) the large number of CH units, which facilitate the formation of C–H···H–C interactions and raise their importance in the total interactions.

In KESZIR (%H···H contacts = 82.5%), the most effective interactions are C–H···S═P HBs, and the CH···HC interactions do not have the major share. However, in BOFHIQ (%H···H contacts = 90.0%), although the C–H···S═P HBs are formed, the share of the CH···HC is much higher than HBs. The effect of H···H contacts can be investigated by a closer look at two molecular pairs in BOFHIQ with the highest total energies (Fig. S9†).

In the first pair (E_{tot} = −34.6 kJ mol^{-1}, BOFHIQ*a*), the most important interactions are two symmetrically equivalent C–H···S═P HBs with a H···S distance of 3.20 Å (3.12 Å considering the neutron-normalized H atom position). The closest CH···HC interaction between two piperidinyl rings has a H···H distance of 2.54 Å in X-ray (2.44 Å normalized value in Hirshfeld). The second pair (E_{tot} = −34.4 kJ mol^{-1}, BOFHIQ*b*) merely includes the homopolar CH···HC interaction. Indeed, in this structure, the P═S acceptor has approximately the same tendency to form hydrogen bonding interactions with different CH donor groups. In such conditions, HBs lose their determinative role in molecular assembly, and the molecules are arranged in a way to form more and stronger CH···HC interactions.

Another noteworthy point that can be mentioned here is revealed by comparing the %H···H contacts of **IV** and BOFHIQ. The contribution rate (energetically) of the CH···HC interactions does not necessarily increase with raising the

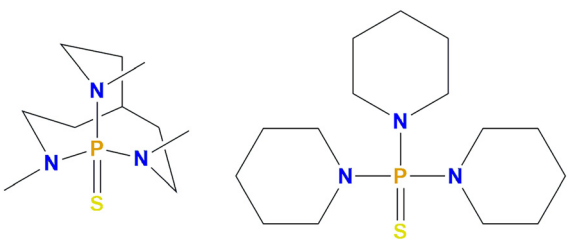

Chart 2 Chemical structures of KESZIR (left) and BOFHIQ (right).

percentage of H···H contacts, and some other factors such as supramolecular assembly and the shape of the substituents have a great impact. In structure **IV**, N–H···S=P HB has the main role in the arrangement of the molecules in one direction, and the molecular packing is not optimized for the formation of stronger homopolar dihydrogen interactions. It also seems that the shape of the *tert*-butylamine substituent is not suitable for establishing strong and numerous interactions, while the piperidinyl rings stack well together. It is manifested in BOFHIQ that the shape of three piperidinyl rings helps the molecules form a denser packing, with stronger CH···HC interactions and higher repulsion forces (Fig. 5).

Repulsion forces. In crystal structures, repulsion forces are enhanced by reducing the distances between molecules. Accordingly, in the studied molecular pairs, the highest repulsion energies are in the pairs with the lowest distances and highest total energy (hydrogen-bonded pairs). In addition, NCI plots demonstrate strong repulsion forces arising from electron-rich atoms in these pairs (*e.g.*, HB acceptors). The repulsion especially increases where two HB acceptors approach and repel each other (as can be seen in pairs **I*a***, and **V*b***).

NCI plots represent that although the decrease in the angle between the two aromatic rings leads to an increase in the area of attraction interactions, it also causes mutual repulsion of π-clouds, which is reflected in repulsion energy values. For instance, in pairs **I*d*** and **I*e***, the interactions are almost the same, but the greater angle between two aromatic rings involved in π···π interaction in **I*e*** leads to the reduction of repulsion force, which is manifested in both NCI plots and values of E_{rep}.

Spectroscopy

The spectroscopy of compound **V** was studied in the literature presented by Yadav *et al.*[26] In the IR spectra, the bands centered at 1180, 1207, and 1230 cm^{-1} for **I**, **II**, and **III** and at 648 cm^{-1} for **IV** are assigned to the P=O and P=S stretching frequencies, respectively. The N–H bands of **I**, **II**, and **IV** appear at 3116, 3240, and 3367 cm^{-1}, respectively.

The phosphorus signal ($^{31}P\{^1H\}$ NMR) appears as a singlet: at −7.40 ppm for amidophosphodiester **I**, 10.90 and 15.07 ppm for diamidophosphoesters **II** and **III**, and 46.74 and 40.67 ppm for phosphorothioic triamides **IV** and **V**.[26] In the ^1H NMR spectra, while the NH units of **II** and **IV** show coupling with phosphorus, compound **I** reveals a singlet for NH. Besides the anisotropic effect of the arene ring, the higher frequency of this signal in **I** (9.67 ppm), with respect to the ones for **II** (4.62 ppm) and **IV** (3.13 ppm), and also its broad fashion (the width at half-maximum of the peak = 21.1 Hz), may be a sign of remaining hydrogen bonding in the solution phase. The triplet fine structure of NH in (**II**) arises from geminal P–H and vicinal H–H couplings (appearance J = 10.4 Hz), and the NH group of **IV** appears as a doublet (J = 8.8 Hz). The methyl proton of the $N(CH_3)(C_6H_{11})$ group (**III**) also shows coupling with phosphorus ($^3J_{P-H}$ = 10.4 Hz).

For **I**, the *ipso*- and *ortho*-carbon atoms (^{13}C NMR) of both NC_5H_4NH and OC_6H_5 groups reveal the couplings with phosphorus (^2J, ^3J). Comparison with analogous compounds shows that the doublets at 150.82 ppm ($^2J_{P-C}$ = 6.5 Hz) and 120.85 ppm ($^3J_{P-C}$ = 4.7 Hz) are related to the phenyl ring and the doublets at 153.95 ppm ($^2J_{P-C}$ = 2.0 Hz) and 112.21 ppm ($^3J_{P-C}$ = 8.9 Hz) are related to the pyridyl ring. A typical example of an analogous compound is $(C_6H_5O)_2P(O)(NH–R–(+)CH(CH_3)(C_6H_5))$, with similar doublets of 150.70/150.57 ppm (J = 6.5 Hz for both) and 120.14/120.13 ppm (J = 4.8 Hz for both).[37] The reason for the appearance of two signals for both *ipso*- and *ortho*-carbon atoms of the literature structure is the presence of a chiral moiety and the diastereotopic relation of phenoxy groups. In compound **IV**, the carbon atoms with two- and three-bond separations from phosphorus also reveal the couplings, with $|^2J_{P-C}| < |^3J_{P-C}|$ (1.0 and 4.5 Hz). For compounds **II** and **III**, some of the carbon atoms with two- and three-bond separations from phosphorus show similar couplings, with the values comparable to the analogous compounds.[38] The $^2J_{P-C}$ and $^3J_{P-C}$ coupling constants of 4-Cl–C_6H_4O moieties are almost similar to the ones of the C_6H_5O moiety in compound **I**: 6.2/5.0 Hz (151.32/122.56 ppm) for **II** and 5.9/4.6 Hz (150.54/122.57 ppm) for **III**.

Experimental

Preparation of $(C_6H_5O)_2P(O)(2\text{-}NHC_5H_4N)$ (I)

To a solution of diphenyl phosphoryl chloride (2.05 mmol) in dry CH_3CN (5 ml), a solution containing 2-aminopyridine (2.05 mmol) and triethylamine (2.05 mmol) in dry CH_3CN (10 ml) was added dropwise at 0 °C. After stirring for 4 h, the solvent was evaporated in a vacuum, and the solid obtained was washed with distilled water. Single crystals were obtained from a solution of the product in CH_3CN/CH_3OH (4 : 1 v/v) after slow evaporation at room temperature.

M.p. = 135 °C. Anal. calc. for $C_{17}H_{15}N_2O_3P$ (326.29): C, 62.58; H, 4.63; N, 8.59. Found: C, 62.81; H, 4.52; N, 8.39. IR (KBr disc, ν, cm^{-1}): 3510, 3466, 3116, 3049, 2886, 2810, 2743, 2685, 1960, 1594, 1431, 1303, 1281, 1180, 1060, 989, 939, 762, 684. $^{31}P\{^1H\}$ NMR (121.77 MHz, DMSO-d_6), δ (ppm): −7.40. ^1H NMR (300.81 MHz, DMSO-d_6), δ (ppm): 9.67 (s, 1H), 8.32 (dd, J_{H-H} = 5.3, 2.0 Hz, 1H), 7.69 (t, J_{H-H} = 7.8 Hz, 1H), 7.43–7.31 (m, 8H), 7.21 (t, J_{H-H} = 7.2 Hz, 2H), 7.11 (d, J_{H-H} = 8.1 Hz, 1H), 6.97 (dd, J_{H-H} = 7.4, 5.0 Hz, 1H). $^{13}C\{^1H\}$ NMR (75.65 MHz, DMSO-d_6), δ (ppm): 153.95 (d, $^2J_{P-C}$ = 2.0 Hz), 150.82 (d, $^2J_{P-C}$ = 6.5 Hz), 148.14, 138.84, 130.32, 125.63, 120.85 (d, $^3J_{P-C}$ = 4.7 Hz), 117.71, 112.21 (*d*, $^3J_{P-C}$ = 8.9 Hz).

Preparation of $(4\text{-}Cl–C_6H_4O)P(O)(NHC_6H_{11})_2$ (II) and $(4\text{-}Cl–C_6H_4O)P(O)(N(CH_3)(C_6H_{11}))_2$ (III)

To a solution of 4-chlorophenyl dichlorophosphate (5 mmol) in dry CH_3CN (10 ml), a solution of amine (20 mmol, cyclohexylamine for **II** and *N*-methylcyclohexylamine for **III**)

in the same solvent (10 ml) was added dropwise at 0 °C. After stirring for 6 h, the solvent was evaporated in a vacuum. The solid obtained was washed with distilled water. Single crystals were obtained from a DMF solution for **II** and CH_3CN for **III**.

(II). M.p. = 98 °C. Anal. calc. for $C_{18}H_{28}ClN_2O_2P$ (370.85): C, 58.30; H, 7.61; N, 7.55. Found: C, 58.07; H, 7.68; N, 7.45. IR (KBr disc, ν, cm^{-1}): 3418, 3240, 2928, 2854, 1620, 1489, 1442, 1207, 1092, 891, 837. $^{31}P\{^1H\}$ NMR (DMSO-d_6, 161.97 MHz), δ (ppm): 10.90 (s). ^1H NMR (400.13 MHz, DMSO-d_6), δ (ppm): 7.37 (d, J = 8.8 Hz, 2H), 7.19 (d, J = 8.0 Hz, 2H), 4.62 (t, J = 10.4 Hz, 2H), 2.87 (m, 2H), 1.77–1.49 (m, 10H), 1.20–1.12 (m, 10H). $^{13}C\{^1H\}$ NMR (100.61 MHz, DMSO-d_6), δ (ppm): 151.32 (d, $^2J_{P-C}$ = 6.2 Hz), 129.50, 127.64, 122.56 (d, $^3J_{P-C}$ = 5.0 Hz), 50.52, 35.72 (d, $^3J_{P-C}$ = 5.1 Hz), 35.60 (d, $^3J_{P-C}$ = 5.1 Hz), 25.63, 25.45.

(III). M.p. = 77 °C. Anal. calc. for $C_{20}H_{32}ClN_2O_2P$ (398.90): C, 60.22; H, 8.08; N, 7.02. Found: C, 60.03; H, 8.12; N, 7.10. IR (KBr disc, ν, cm^{-1}): 3047, 2928, 2854, 1589, 1485, 1446, 1385, 1338, 1230, 1122, 1092, 984, 895, 771. $^{31}P\{^1H\}$ NMR (161.97 MHz, DMSO-d_6), δ (ppm): 15.07 (s). ^1H NMR (400.13 MHz, DMSO-d_6), δ (ppm): 7.40 (d, J_{H-H} = 6.8 Hz, 2H), 7.19 (d, J_{H-H} = 8.8 Hz, 2H), 3.24 (m, 2H), 2.51 (d, J_{P-H} = 10.4 Hz, 6H), 1.72 (m, 4H), 1.47 (m, 10H), 1.22 (m, 4H), 1.02 (m, 2H). $^{13}C\{^1H\}$ NMR (100.61 MHz, DMSO-d_6), δ (ppm): 150.54 (d, $^2J_{P-C}$ = 5.9 Hz), 129.81, 128.34, 122.57 (d, $^3J_{P-C}$ = 4.6 Hz), 54.97 (d, J = 4.2 Hz), 30.68, 30.65, 27.92 (d, J_{P-C} = 3.9 Hz), 26.04, 26.02, 25.46.

Preparation of $P(S)[NHC(CH_3)_3]_3$ (IV)

To a solution of thiophosphoryl chloride (10 mmol) in dry CH_3CN (10 ml), a solution of *tert*-butylamine (60 mmol) in the same solvent (10 ml) was added at 0 °C. After stirring for 6 hours, the solvent was evaporated at room temperature, and the residual solid was washed with distilled water. Single crystals suitable for X-ray crystallography were obtained from a CH_3CN/CH_3OH (1 : 1 v/v) mixture after slow evaporation at room temperature.

M.p. = 132 °C. Anal. calc. for $C_{12}H_{30}N_3PS$ (279.42): C, 51.58; H, 10.82; N, 15.04; S, 11.48. Found: C, 51.21; H, 10.94; N, 15.18; S, 11.55. IR (KBr disc, ν, cm^{-1}): 3398, 3367, 2970, 2966, 1473, 1377, 1223, 1007, 852, 752, 648, 594. $^{31}P\{^1H\}$ NMR (121.50 MHz, DMSO-d_6), δ (ppm): 46.74 (s). ^1H NMR (300.13 MHz, DMSO-d_6), δ (ppm): 3.13 (d, $^2J_{P-H}$ = 8.8 Hz, 3H), 1.30 (m, 27H). $^{13}C\{^1H\}$ NMR (75.47 MHz, DMSO-d_6), δ (ppm): 51.23 (d, $^2J_{P-C}$ = 1.0 Hz), 31.02 (d, $^3J_{P-C}$ = 4.5 Hz).

Preparation of $P(S)(3\text{-}NHC_5H_4N)_3$ (V)

The preparation method and characterization of compound **V** have been reported in the literature.[26,39] The synthesis procedure reported here is similar to the literature method with a few modifications in solvent and temperature (dry toluene and reflux conditions in the literature). For the synthesis of **V**, to a solution of thiophosphoryl chloride in dry $CHCl_3$, a solution of 3-aminopyridine and triethylamine (1 : 3 : 3 mole ratio) in the same solvent was added at 0 °C. After 4 h of stirring, the solvent was removed in a vacuum and the obtained solid was washed with distilled water to remove triethylamine hydrochloride. The crystals, suitable for X-ray analysis, were obtained from a mixture of $CHCl_3/CH_3OH$ (1 : 1 v/v) after slow evaporation at room temperature.

Crystal structure determination and theoretical methods

Diffraction data were collected on Rigaku/Oxford Diffraction diffractometers using Mo Kα (**I**, **IV**, **V**) and Cu Kα (**II**, **III**) radiation at 173 K (**I**), 120 K (**II**, **IV**, **V**), and 293 K (**III**). The structures were solved either by direct methods (**I**, **IV**, **V**) or charge-flipping algorithm (**II**, **III**), and refined by full-matrix least-squares methods on either F (**II**, **III**) or F^2 (**I**, **IV**, **V**). All non-hydrogen atoms were refined anisotropically, and carbon-bonded hydrogen atoms were refined as riding on their carrier atoms, using constraints on the geometrical and displacement parameters. Nitrogen-bonded hydrogen atoms were either refined freely (**I**), by using distance restraints (**II**), or full geometry constraints (**IV**, **V**), with the isotropic displacement parameters set to $1.2U_{eq}$ of the parent atom (**II**, **IV**, **V**). Structure **IV** was refined as an inversion twin (Flack parameter 0.41(13)).

To make an accurate description of the crystal packing, crystal lattice energy calculations were performed using CrystalExplorer 17.5 software with the basis set CE-B3LYP/6-31G(d,p) based on the molecular shell considering the first sphere of neighboring molecules. In this method, the interaction energy of each molecular pair [E_{tot}] is expressed as:

$$E_{tot} = k_{ele}E_{ele} + k_{pol}E_{pol} + k_{dis}E_{dis} + k_{rep}E_{rep}$$

where E_{ele}, E_{pol}, E_{dis}, and E_{rep} are electrostatic, polarization, dispersion, and repulsion energy, respectively, and k constants are scale factors, whose values are given in Table S23.† In this expression, the total interaction energy is constructed from its individual components rather than breaking down a much larger total energy. The definition of each term is presented in relevant literature.[40,41] Crystal lattice energies (E_{latt}) are calculated using the formula $E_{latt} = \frac{1}{2}\sum N \cdot E_{tot}$,[41] ($N$ is the number of equivalent pair(s) with the same energy values in the molecular shell), and interactions with further molecules are ignored. Similar formulas were applied to calculate the sum of each energy component ($E_X^* = \frac{1}{2}\sum N \cdot E_X$, where X = electrostatic, dispersion, polarization, and repulsion components. The obtained results are used in Fig. 5). The calculated energy frameworks and 2D fingerprint plots were also generated.[42–44]

Every point in the fingerprint plots represents the distances from each point on the Hirshfeld surface to the internal nearest atom (d_i) and external nearest atom (d_e).

Therefore, the term $d_i + d_e$ can be an evaluation criterion for the bond strength.

To detect the most important intermolecular interactions in the crystal lattice, QTAIM analysis[45] and non-covalent interaction (NCI)[46] plots are implemented for the molecular pairs with total energies stronger than −20 kJ mol^{-1}. For this purpose, energy calculations were performed at the M06-2X/6-311G(d,p) level of theory using Gaussian 09 (ref. 47) for selected molecular pairs with both neutron-normalized and original X-ray hydrogen atom positions. The energy calculations were also carried out with neutron-normalized hydrogen positions at the M06-2X/6-311++G(d,p) level of theory. The NCI and QTAIM calculations were performed using the MultiWFN program package,[48] and selected topological parameters including potential energy density ($V(r)$), kinetic energy density ($G(r)$), total electronic density ($\rho(r)$), and its corresponding Laplacian ($\nabla^2\rho(r)$) at the BCPs of interactions are reported in Tables 2 and S16–S19.† Moreover, the energy value of each interaction is estimated using the Espinosa relationship ($E_{Esp} = V(r)/2$)[49] and reported in these tables.

An overview of E_{Esp} and E_{tot}

The Espinosa–Molins–Lecomte estimation of energy (E_{Esp}) is applied to study the strengths of interactions in various crystal and computed structures. The crystal lattice energy calculation provides the total energy in a molecular pair (E_{tot}), which includes some divided intermolecular contacts. Good accuracy of crystal lattice energy calculations was approved with the results obtained from sublimation enthalpies.[50] Spackman *et al.* examined the energy estimation for divided contacts by considering the experimental electron density for the topological analysis. They also compared E_{tot} with the sum of the E_{Esp} energies for BCPs in a pair and showed their discrepancies by a scatter plot.[51]

Here the crystal lattice energies of new structures (**I**) to (**V**) were computed, and then the generated neutron-normalized structures were considered for the topological calculations based on the theoretical electron density. The topological analyses based on the original X-ray data are also given for comparison. The potential energy densities ($V(r)$) of the BCPs are also used to compare the strengths of interactions.

Conclusions

Designing new phosphoramide and thiophosphoramide structures and X-ray crystallography experiments combined with chemical calculations provide an opportunity to study the geometry and energy estimation of moderate NH⋯X (X = O, N) and weak NH⋯S, CH⋯Y (Y = S, O, Cl, N, π), H⋯H and π⋯π interactions/contacts. The new structures have P(O)(N)(O)$_2$, P(O)(O)(N)$_2$, and P(S)(N)$_3$ cores. One of the new structures with a P(O)(O)(N)$_2$ skeleton includes a classical (NH⋯)$_2$O═P grouping and the other one lacks an NH unit to prevent the formation of a classical hydrogen bond. In the presence of strong hydrogen bonds, the significance of weaker hydrogen bonds decreases. Typical are the CH⋯Cl/NH⋯O hydrogen bonds in structure **II**, where the CH⋯Cl makes the structure more stable but has no remarkable effect on the molecular arrangement. Two new structures with a P(S)(N)$_3$ skeleton (including three NH units) and with different numbers of possible acceptor sites were studied, and two other structures (without any NH unit) were retrieved from the Cambridge Structural Database (CSD) for the study of competition between H⋯H and H⋯S contacts. The homopolar CH⋯HC interactions, especially in the compounds with large alkyl fragments, have a significant impact on the stabilization of the structures. Comparative surveys of our structures with selected structures from the CSD show that the role of the H⋯H interactions can be determinative when the three following conditions are met. First, the HBs are weak. Second, the alkyl fragments comprise most of the molecular volume. Third, the shape of the alkyl fragment is convenient for approaching hydrogens together in the packing. The shape of the cyclohexyl substituents facilitates their regular arrangement in the structure and strengthens the interactions between them. The low Lewis-based characteristics of the ester oxygen atom and amide N atom in amidophosphoester and thiophosphoramide structures were confirmed, which are reflected in their low acceptor capabilities and the estimated energies of contacts formed. The contacts of saturated and unsaturated rings were evaluated. The arene rings are arranged through the π⋯π and CH⋯π interactions, and the number of attractive interactions is enhanced when a cyclohexyl ring is faced with an arene ring, owing to the increase in the number of CH⋯π interactions. In the new structures investigated, the pyridine nitrogen atom is the successful competitor in the presence of other acceptor groups, such as P═O and P═S. Calculated energy frameworks indicate that the intermolecular interactions between the hydrogen-bonded pairs play the main role in the formation of the crystal structures, due to their higher total energy values (E_{tot}).

Conflicts of interest

There are no conflicts to declare.

Acknowledgements

Financial support for this work by the Ferdowsi University of Mashhad is gratefully acknowledged (Project No. 56293/3). We acknowledge the X-ray Diffraction and Bio-SAXS Core Facility of CIISB, Instruct-CZ Centre, supported by MEYS CR (LM2018127), and the infrastructure Czech Nanolab (LM2023051). The authors appreciatively acknowledge the Cambridge Crystallographic Data Centre for access to the CSD Enterprise suite.

Notes and references

1 A. J. Cruz-Cabeza, S. M. Reutzel-Edens and J. Bernstein, *Chem. Soc. Rev.*, 2015, **44**, 8619–8635.

2 N. Blagden and R. J. Davey, *Cryst. Growth Des.*, 2003, **3**, 873–885.

3 G. R. Desiraju, J. J. Vittal and A. Ramanan, *Crystal Engineering: A Textbook*, Co-Published with Indian Institute of Science (IISc), Bangalore, India, 2011.
4 S. Parveen, R. J. Davey, G. Dent and R. G. Pritchard, *Chem. Commun.*, 2005, 1531–1533.
5 J. Nývlt, *Cryst. Res. Technol.*, 1995, **30**, 443–449.
6 G. R. Desiraju, *J. Am. Chem. Soc.*, 2013, **135**, 9952–9967.
7 G. Cavallo, P. Metrangolo, R. Milani, T. Pilati, A. Priimagi, G. Resnati and G. Terraneo, *Chem. Rev.*, 2016, **116**, 2478–2601.
8 C. B. Aakeröy and K. R. Seddon, *Chem. Soc. Rev.*, 1993, **22**, 397–407.
9 C. B. Aakeröy, S. Panikkattu, P. D. Chopade and J. Desper, *CrystEngComm*, 2013, **15**, 3125–3136.
10 L. R. Nassimbeni, N. B. Báthori, L. D. Patel, H. Su and E. Weber, *Chem. Commun.*, 2015, **51**, 3627–3629.
11 S. Bhandary, A. Sirohiwal, R. Kadu, S. Kumar and D. Chopra, *Cryst. Growth Des.*, 2018, **18**, 3734–3739.
12 A. G. P. Maloney, P. A. Wood and S. Parsons, *CrystEngComm*, 2014, **16**, 3867–3882.
13 C. F. Matta, J. Hernández-Trujillo, T.-H. Tang and R. F. W. Bader, *Chem. – Eur. J.*, 2003, **9**, 1940–1951.
14 A. A. Fokin, D. Gerbig and P. R. Schreiner, *J. Am. Chem. Soc.*, 2011, **133**, 20036–20039.
15 M. Alonso, T. Woller, F. J. Martín-Martínez, J. Contreras-García, P. Geerlings and F. De Proft, *Chem. – Eur. J.*, 2014, **20**, 4931–4941.
16 E. M. Cabaleiro-Lago and J. Rodríguez-Otero, *ACS Omega*, 2018, **3**, 9348–9359.
17 C. Wang, Y. Mo, J. P. Wagner, P. R. Schreiner, E. D. Jemmis, D. Danovich and S. Shaik, *J. Chem. Theory Comput.*, 2015, **11**, 1621–1630.
18 F. M. Oliveira, L. C. A. Barbosa and F. M. D. Ismail, *RSC Adv.*, 2014, **4**, 18998–19012.
19 *Handbook of pesticides: methods of pesticide residues analysis*, ed. L. M. L. Nollet and H. S. Rathore, CRC Press, Boca Raton, Fla., 2010.
20 D. A. Safin, M. G. Babashkina, M. Bolte and Y. Garcia, *CrystEngComm*, 2012, **14**, 774–778.
21 M. Bortoluzzi, J. Castro, A. D. Vera, A. Palù and V. Ferraro, *New J. Chem.*, 2021, **45**, 12871–12878.
22 M. Pourayoubi, M. Toghraee, J. Zhu, M. Dušek, P. J. Bereciartua and V. Eigner, *CrystEngComm*, 2014, **16**, 10870–10887.
23 F. Hamzehee, M. Pourayoubi, M. Nečas and D. Choquesillo-Lazarte, *Acta Crystallogr., Sect. C: Struct. Chem.*, 2017, **73**, 287–297.
24 M. Pourayoubi, M. Abrishami, V. Eigner, M. Nečas, M. Dušek and M. Delavar, *Acta Crystallogr., Sect. C: Struct. Chem.*, 2014, **70**, 1147–1152.
25 M. Pourayoubi, J. P. Jasinski, S. Shoghpour Bayraq, H. Eshghi, A. C. Keeley, G. Bruno and H. Amiri Rudbari, *Acta Crystallogr., Sect. C: Cryst. Struct. Commun.*, 2012, **68**, o399–o404.
26 A. Yadav, A. K. Srivastava, P. Kulkarni, P. Divya, A. Steiner, B. Praveenkumar and R. Boomishankar, *J. Mater. Chem. C*, 2017, **5**, 10624–10629.
27 T. Steiner, *Angew. Chem., Int. Ed.*, 2002, **41**, 48–76.
28 K. S. Kim, S. Karthikeyan and N. J. Singh, *J. Chem. Theory Comput.*, 2011, **7**, 3471–3477.
29 D. B. Ninković, D. Z. Vojislavljević-Vasilev, V. B. Medaković, M. B. Hall, E. N. Brothers and S. D. Zarić, *Phys. Chem. Chem. Phys.*, 2016, **18**, 25791–25795.
30 D. Danovich, S. Shaik, F. Neese, J. Echeverría, G. Aullón and S. Alvarez, *J. Chem. Theory Comput.*, 2013, **9**, 1977–1991.
31 L. R. de Almeida, P. S. Carvalho, H. B. Napolitano, S. S. Oliveira, A. J. Camargo, A. S. Figueredo, G. L. B. de Aquino and V. H. Carvalho-Silva, *Cryst. Growth Des.*, 2017, **17**, 5145–5153.
32 J. Echeverría, G. Aullón, D. Danovich, S. Shaik and S. Alvarez, *Nat. Chem.*, 2011, **3**, 323–330.
33 A. Ruiz, H. Pérez, C. Morera-Boado, L. Almagro, C. C. P. da Silva, J. Ellena, J. M. G. de la Vega, R. Martínez-Álvarez, M. Suárez and N. Martín, *CrystEngComm*, 2014, **16**, 7802–7814.
34 C. R. Groom, I. J. Bruno, M. P. Lightfoot and S. C. Ward, *Acta Crystallogr., Sect. B: Struct. Sci., Cryst. Eng. Mater.*, 2016, **72**, 171–179.
35 M. Rudd, S. Lindeman and S. Husebye, *Acta Chem. Scand.*, 1996, **50**, 759–774.
36 M. Taherzadeh, M. Pourayoubi and M. Nečas, *Phosphorus, Sulfur Silicon Relat. Elem.*, 2019, **194**, 39–46.
37 F. Sabbaghi, M. Pourayoubi, M. Nečas and K. Damodaran, *Acta Crystallogr., Sect. C: Struct. Chem.*, 2019, **75**, 77–84.
38 M. Toghraee, M. Pourayoubi and V. Divjakovic, *Polyhedron*, 2011, **30**, 1680–1690.
39 A. Yadav, A. K. Srivastava, A. Balamurugan and R. Boomishankar, *Dalton Trans.*, 2014, **43**, 8166–8169.
40 M. J. Turner, S. Grabowsky, D. Jayatilaka and M. A. Spackman, *J. Phys. Chem. Lett.*, 2014, **5**, 4249–4255.
41 M. A. Spackman, *CrystEngComm*, 2018, **20**, 5340–5347.
42 M. J. Turner, J. J. McKinnon, S. K. Wolff, D. J. Grimwood, P. R. Spackman, D. Jayatilaka and M. A. Spackman, *CrystalExplorer (version 17)*, University of Western Australia, 2017.
43 C. F. Mackenzie, P. R. Spackman, D. Jayatilaka and M. A. Spackman, *IUCrJ*, 2017, **4**, 575–587.
44 M. A. Spackman and J. J. McKinnon, *CrystEngComm*, 2002, **4**, 378–392.
45 R. F. W. Bader, *Atoms in Molecules: A Quantum Theory*, Oxford University Press, Oxford, New York, 1994.
46 E. R. Johnson, S. Keinan, P. Mori-Sánchez, J. Contreras-García, A. J. Cohen and W. Yang, *J. Am. Chem. Soc.*, 2010, **132**, 6498–6506.
47 M. J. Frisch, *et al.*, *GAUSSIAN09*, Gaussian Inc., Wallingford, CT, USA.
48 T. Lu and F. Chen, *J. Comput. Chem.*, 2012, **33**, 580–592.
49 E. Espinosa, E. Molins and C. Lecomte, *Chem. Phys. Lett.*, 1998, **285**, 170–173.
50 S. P. Thomas, P. R. Spackman, D. Jayatilaka and M. A. Spackman, *J. Chem. Theory Comput.*, 2018, **14**, 1614–1623.
51 M. A. Spackman, *Cryst. Growth Des.*, 2015, **15**, 5624–5628.